Magnetic rotation in ^{82}Rb and ^{84}Rb

R. Schwengner,[1] G. Rainovski,[1,2] H. Schnare,[1] A. Wagner,[1] F. Dönau,[1] A. Jungclaus,[3] M. Hausmann,[4] O. Iordanov,[4] K. P. Lieb,[4] D. R. Napoli,[5] G. de Angelis,[5] M. Axiotis,[5] N. Marginean,[5,*] F. Brandolini,[6] and C. Rossi Alvarez[6]

[1]*Institut für Kern- und Hadronenphysik, Forschungszentrum Rossendorf, D-01314 Dresden, Germany*

[2]*Faculty of Physics, University of Sofia, 1164 Sofia, Bulgaria*

[3]*Instituto de Estructura de la Materia, Consejo Superior de Investigaciones Científicas, E-28006 Madrid, and Departamento de Física Teórica, Universidad Autónoma de Madrid, E-28049 Madrid, Spain*

[4]*II. Physikalisches Institut, Universität Göttingen, D-37073 Göttingen, Germany*

[5]*INFN, Laboratori Nazionali di Legnaro, I-35020 Legnaro, Italy*

[6]*INFN and Dipartimento di Fisica dell'Università di Padova, I-35131 Padova, Italy*

(Received 5 April 2002; published 6 August 2002)

High-spin states in ^{82}Rb and ^{84}Rb were populated in the reaction ^{11}B + ^{76}Ge at beam energies of 45 and 50 MeV. γ rays were detected with the spectrometer GASP. The level schemes of ^{82}Rb and ^{84}Rb were extended up to 6.0 and 7.4 MeV, respectively. Mean lifetimes of five levels in ^{82}Rb and 11 levels in ^{84}Rb were determined using the Doppler-shift-attenuation method. Regular magnetic dipole bands including strong $M1$ and weak $E2$ transitions observed in both nuclei show the characteristic features of magnetic rotation. These bands have been successfully described in the tilted-axis cranking model on the basis of the four-quasiparticle configuration $\pi(fp)\ \pi(g_{9/2}^2)\ \nu(g_{9/2})$. The calculations reproduce the band-like properties as well as absolute $B(M1)$ and $B(E2)$ transition strengths in both nuclei, which supports the concept of magnetic rotation. Excited states in ^{84}Rb were also interpreted in terms of the shell model using the model space $\pi(0f_{5/2},1p_{3/2},1p_{1/2},0g_{9/2})\ \nu(1p_{1/2},0g_{9/2})$. The predictions for low-lying states agree in general with the experiment. Moreover, calculated states with the main configuration $\pi(0f_{5/2}^{-2}1p_{3/2}^{-1}0g_{9/2}^2)\ \nu(0g_{9/2}^{-3})$ can be combined into $M1$ sequences which reproduce roughly the experimental transition strengths. However, these sequences do not show the features of magnetic rotation such as regular level spacings and $B(M1)$ values which decrease with increasing rotational frequency.

DOI: 10.1103/PhysRevC.66.024310 PACS number(s): 23.20.Lv, 25.85.Ge, 27.50.+e

I. INTRODUCTION

Magnetic rotation, a novel kind of nuclear rotation, has attracted great interest in recent years. After the first observation of regular magnetic dipole ($M1$) bands in nearly spherical Pb isotopes [1–9], these so-called shears bands were described in the tilted-axis-cranking (TAC) model [10] and were predicted to exist also in other regions of the nuclear chart [11,12]. Indeed, magnetic rotation was observed in the predicted regions around $A=110$ [13–17] and $A=140$ [18].

In order to search for magnetic rotation in the mass region around $A=80$ we studied the odd-odd isotopes $^{82}Rb_{45}$ and $^{84}Rb_{47}$ and found $M1$ bands in each of these nuclei [19,20]. These $M1$ bands follow the regular rotational behavior [$E \sim J(J+1)$, i.e., $E_\gamma^{M1}=\hbar\omega\sim J$]. The $B(M1)/B(E2)$ ratios determined from branching ratios of transitions within the $M1$ bands reach values up to 25 $(\mu_N/e\,\mathrm{b})^2$ and decrease smoothly with increasing spin in the range of $13\leqslant J\leqslant 16$. This behavior is typical for magnetic rotation and caused by the gradual alignment of the spins of the involved proton and neutron orbitals (shears mechanism). We described the regular negative-parity $M1$ bands in ^{82}Rb and ^{84}Rb within the TAC model on the basis of the lowest-lying four-quasiparticle ($4qp$) configuration with negative parity $\pi(fp)\ \pi(g_{9/2}^2)\ \nu(g_{9/2})$ [19]. The good agreement between experimental and calculated characteristics proves the concept of magnetic rotation for these bands.

So far, our interpretation of the $M1$ bands in ^{82}Rb and ^{84}Rb was based on $B(M1)/B(E2)$ ratios deduced from γ-ray intensities only. However, a more detailed test of the predictions of the TAC model requires also the knowledge of absolute $M1$ and $E2$ transition strengths. Therefore, the present work focuses on the determination of level lifetimes by applying the Doppler-shift-attenuation (DSA) method. This paper compiles all the experimental information deduced from our experiments and complements the preceding publications on the thin-target experiment [19,20].

II. EXPERIMENTAL METHODS AND RESULTS

Excited states of ^{82}Rb and ^{84}Rb were populated via the reactions ^{76}Ge(^{11}B,5n) and ^{76}Ge(^{11}B,3n), respectively, using the ^{11}B beam of the XTU tandem accelerator of the Laboratori Nazionali di Legnaro. γ rays were detected with the GASP spectrometer [21] consisting of 40 escape-suppressed HPGe detectors and an inner ball containing 80 BGO elements. In the first of the two experiments [19,20] the beam energy was 50 MeV. A thin target consisting of a stack of two self-supporting ^{76}Ge foils enriched to 92.8 % with a thickness of 0.2 mg cm^{-2} each was used. Approximately 1.5×10^8 γ-γ-γ coincidence events were collected

*On leave from NIPNE Bucharest, Romania.

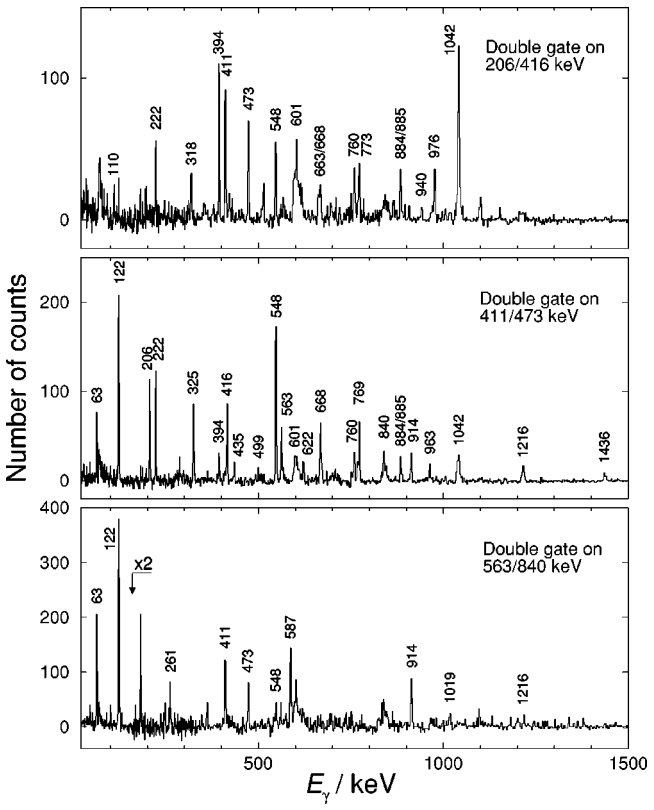

FIG. 1. Examples of doubly gated coincidence spectra. Transitions assigned to ^{82}Rb are marked with their energies in keV.

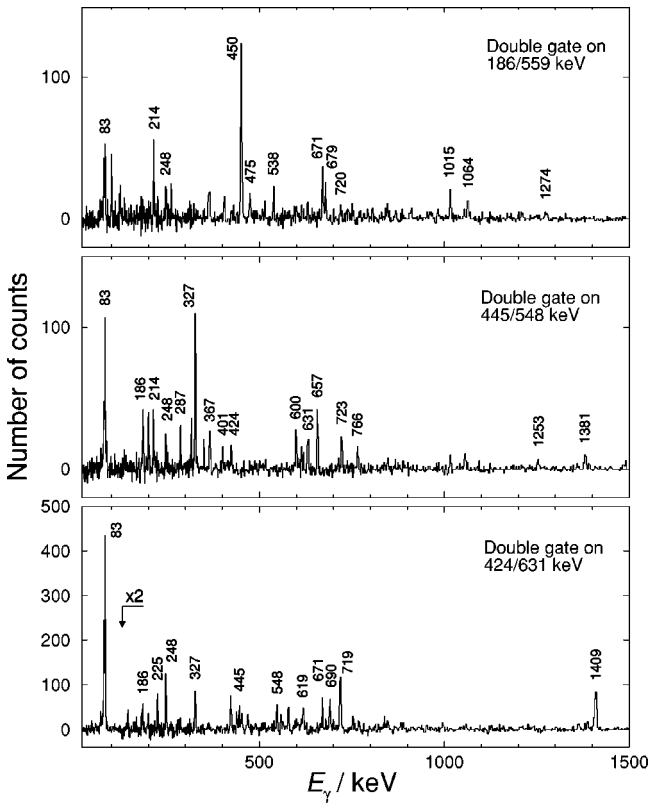

FIG. 2. Examples of doubly gated coincidence spectra. Transitions assigned to ^{84}Rb are marked with their energies in keV.

and sorted off-line into E_γ-E_γ matrices as well as an E_γ-E_γ-E_γ cube. The beam energy in the second experiment was 45 MeV. The target consisted of a 1.2 mg cm^{-2} thick layer of ^{76}Ge evaporated onto a 3 mg cm^{-2} tantalum backing. A total of 2×10^9 γ-γ coincidence events were measured and sorted off-line into E_γ-E_γ matrices. Coincidence spectra were extracted by setting gates on appropriate peak and background intervals in the cube and the matrices using the RADWARE package [22] and the code VS [23], respectively. Examples of doubly gated background-corrected coincidence spectra extracted from the cube are shown in Figs. 1 and 2. The γ rays assigned to ^{82}Rb and ^{84}Rb on the basis of the present coincidence experiments are compiled in Tables I and II.

A. γ-γ directional correlations

The analysis of directional correlations of coincident γ rays emitted from oriented states (DCO) was applied to deduce the multipole orders of the γ rays and thus to assign spins to the emitting states. This method is based on the formalism described in Refs. [24,25] and discussed, e.g., in Ref. [26].

In the present experiment, γ-γ events with one γ ray detected in one of the twelve detectors positioned at angles of 31.7°, 36.0°, 144.0°, and 148.3° (weighted averages 35° or 145°, respectively), and the other one detected in one of the eight detectors at 90° relative to the beam direction were sorted into a coincidence matrix. Coincidence spectra were extracted by setting gates on certain peak and background intervals in the (35°/145°,90°) matrix and in the transposed (90°,35°/145°) matrix. The DCO ratios were obtained as the ratios of peak intensities in both background-corrected spectra. A DCO ratio of 1.0 is expected if the gating and observed transitions are stretched transitions of pure and equal multipole order. For the present detector geometry and completely aligned nuclei, a value of 0.54 is expected for a pure dipole transition gated on a stretched quadrupole transition. Consequently, the inverse value of 1.85 is expected for a quadrupole transition gated on a dipole transition. $E2$ admixtures to $M1$ transitions are assumed if these expected values lie outside the errors of the experimental DCO ratios. The DCO ratios deduced for transitions in ^{82}Rb and ^{84}Rb are listed in Tables I and II.

B. Lifetimes

In order to determine mean lifetimes, Doppler shifts of γ rays observed in coincidence spectra at average angles of 35° and 145° to the beam direction were analyzed by using the DSA method. For this purpose, γ-γ events with one γ ray detected at the average angles of 35° or 145°, respectively, and the other one detected at any angle were sorted into two different matrices. Coincidence spectra at 35° or 145°, respectively, were extracted by setting gates on certain peak and background intervals of the axis including any angle in the two different matrices. The lifetimes were deduced from a comparison of experimental with calculated line shapes. The velocity distributions of the emitting nuclei

TABLE I. γ rays assigned to ^{82}Rb.

E_γ [a] (keV)	I_γ [b]	R_{DCO} [c]	E_γ^{gate} [d] (keV)	$\sigma\lambda$ [e]	J_i^π [f]	J_f^π [g]	E_i [h] (keV)
45.4(9)		1.1(4)	122	$(M1)$ [i]	$8^{(+)}$	$7^{(+)}$	300.7
63.4(1)	86(6)	0.83(4)	122	$(M1)$ [i]	$7^{(+)}$	6^+	254.5
109.8(2)	4.8(3)				9^-	9^-	1842.8
122.4(1)	176(7)			$E1$ [i]	6^+	5^-	190.9
206.4(1)	49(3)	0.87(5)	416	$M1/E2$	7^-	6^-	690.0
222.5(1)	15.5(8)	1.0(1)	411	$(M1)$	11^-	(10^-)	2616.3
261.2(3)	4.5(3)				$12^{(+)}$	(11^+)	2551.0
296.7(2)	8.7(5)	0.4(1)	325	$(M1/E2)$	7^-	(6^-)	690.0
318.3(2)	6.8(5)				12^-	(11^-)	3026.9
325.1(1)	14.1(8)				(6^-)	5^-	393.4
393.9(2)	21(1)	1.1(1)	416	$M1$	8^-	7^-	1083.8
410.6(1)	51(3)	0.9(1)	63/122	$M1$	12^-	11^-	3026.9
415.7(1)	66(19)			$M1$ [i]	6^-	5^-	483.8
417.8(2)	19.4(11)				$10^{(+)}$	$9^{(+)}$	1280.8
434.8(2)	13.9(8)				7^-	$7^{(+)}$	690.0
473.0(1)	41(2)	0.9(1)	63/122	$M1$	13^-	12^-	3499.9
499.1(4)	8.3(6)				7^-	6^+	690.0
547.7(1)	32(2)	1.0(1)	411	$M1$	14^-	13^-	4047.5
559.1(3)	17.6(13)						3518.8
562.6(1)	100(5)	0.59(3)	63/122	$M1/E2$	$9^{(+)}$	$8^{(+)}$	863.2
587.3(2)	15.5(10)				(11^+)	$10^{(+)}$	2289.9
600.8(4)	18.6(1)				8^-	6^-	1083.8
620.7(2)	64(4)	1.1(1)	63/122	$M1$	$11^{(+)}$	$10^{(+)}$	1901.5
621.8(2)	32(5)				7^-	5^-	690.0
631.9(2)	24(2)				$13^{(+)}$	$12^{(+)}$	3182.8
662.6(5)	7.1(5)				(10^-)	9^-	2393.9
668.4(2)	17.8(11)	0.9(2)	411	$M1$	15^-	14^-	4715.8
759.5(2)	24(2)	1.0(1)	416	$M1$	9^-	8^-	1842.8
768.8(5)	9.2(8)				$(16)^-$	15^-	5484.6
773.1(3)	18.1(10)	1.6(2)	416	$E2$	11^-	9^-	2616.3
839.5(2)	61(3)	0.91(6)	63/122	$(M1/E2)$	$10^{(+)}$	$9^{(+)}$	1702.7
865.6(5)	11.7(10)				(11^-)	9^-	2708.6
883.5(9)	7.1(8)				13^-	11^-	3499.9
884.8(5)	9.7(6)				11^-	9^-	2616.3
913.5(2)	17.6(10)	0.9(1)	63/122	$(E1)$	11^-	$10^{(+)}$	2616.3
940.4(8)	6.8(6)				(13^-)	(11^-)	3649.0
963.0(2)	23(2)	1.0(1)	325	$(E2)$	(8^-)	(6^-)	1356.3
976.5(4)	17.6(11)				(11^-)	9^-	2708.6
980.0(2)	73(4)	1.4(1)	63/122	$E2$	$10^{(+)}$	$8^{(+)}$	1280.8
1019.2(6)	10.2(8)				14^-	12^-	4047.5
1037.6(3)	17.8(11)				(10^-)	(8^-)	2393.9
1038.2(5)	14.1(11)				$11^{(+)}$	$9^{(+)}$	1901.5
1041.7(2)	55(3)	1.6(2)	416	$E2$	9^-	7^-	1732.1
1058.1(4)	18.3(13)					$11^{(+)}$	2959.7
1096.9(3)	40(3)					$9^{(+)}$	1960.2
1139.8(9)	7.8(8)					$11^{(+)}$	3041.3
1215.8(5)	11.3(8)				15^-	13^-	4715.8
1270.1(2)	43(2)	1.4(1)	63/122	$E2$	$12^{(+)}$	$10^{(+)}$	2551.0
1281.2(5)	15.7(11)	1.6(2)	63/122	$E2$	$13^{(+)}$	$11^{(+)}$	3182.8
1347.4(6)	11.0(8)				(15^+)	$13^{(+)}$	4530.2
1379.2(11)	4.7(5)					(11^+)	3669.1

TABLE I. (*Continued*).

E_γ [a] (keV)	I_γ [b]	R_{DCO} [c]	E_γ^{gate} [d] (keV)	$\sigma\lambda$ [e]	J_i^π [f]	J_f^π [g]	E_i [h] (keV)
1436.2(6)	9.7(6)				$(16)^-$	14^-	5484.6
1464.8(4)	18.4(1)				(14^+)	$12^{(+)}$	4015.8
1481.5(12)	4.7(5)				(17^+)	(15^+)	6011.7
1573.7(16)	3.4(5)				(16^+)	(14^+)	5589.5

[a]Transition energy. The error in parentheses is given in units of the last digit.
[b]Relative intensity of the γ ray normalized to $I_\gamma = 100$ of the $9^{(+)} \rightarrow 8^{(+)}$ transition at 562.6 keV.
[c]DCO ratio $R_{DCO} = W(90°,35°/145°)/W(35°/145°,90°)$.
[d]Energy of the gating transition used for the determination of the DCO ratio.
[e]Multipolarity compatible with the DCO ratio, the deexcitation mode, and the lifetime of the initial state.
[f]Spin and parity of the initial state.
[g]Spin and parity of the final state.
[h]Energy of the initial state.
[i]Taken from Refs. [31,32].

were calculated with a Monte Carlo code taking into account reactions at different depths in the target, the kinematics of the reaction and the slowing-down and deflection of the recoil nuclei [27]. For the slowing-down process the cross sections given in Ref. [28] were used with correction factors of $f_e = 0.9$ and $f_n = 0.7$ for the electronic and nuclear stopping powers, respectively [29]. In order to deduce the level lifetimes, cascade feeding from all levels observed above the considered one as well as sidefeeding from unobserved levels was taken into account. The sidefeeding times were assumed to be zero for the maximum excitation energies of $E^* = 5.5$ MeV in ^{82}Rb and $E^* = 23$ MeV in ^{84}Rb. These values were derived from the relation $E^* = E^{c.m.}_{^{11}B} + Q - N_n E_n$, where Q and $N_n E_n$ denote the Q value and the mean total energy of the N emitted neutrons, respectively, with values of $Q = -28.7$ MeV, $N_n E_n = 5$ MeV for ^{82}Rb and $Q = -9.0$ MeV, $N_n E_n = 7.5$ MeV for ^{84}Rb. The values of E_n correspond to mean energies of emitted neutrons in different reactions calculated with evaporation codes as described, e.g., in Ref. [30]. With decreasing excitation energy E an increase of the sidefeeding time according to $\tau_{sf} = (E^* - E)/\text{MeV} \cdot 0.03$ ps was assumed [29]. Examples of the line-shape analysis are shown in Fig. 3. The two calculated line shapes corresponding to the complementary observation angles of 35° and 145° were optimized simultaneously in one least-squares fit. This allowed background peaks to be taken into account correctly [see Fig. 3(a)]. For a given transition, different calculations were carried out in which the lifetimes and intensities of the cascade feeding were varied within their errors. In this way the influence of these quantities on the lifetimes and thus, the uncertainties of the lifetimes due to the errors of lifetimes of levels above and intensities of feeding transitions were determined. The influence of variations of the sidefeeding times and intensities on the level lifetimes is negligible compared with the influence of the bigger lifetimes of the feeding levels or the influence due to the uncertainties of the intensities of feeding transitions.

The lifetimes obtained from this analysis are given in Tables III and IV. Transition strengths deduced from these lifetimes are given in Tables V and VI.

III. LEVEL SCHEMES

The level schemes of ^{82}Rb and ^{84}Rb discussed in the following were established in the thin-target experiment [19,20]. These level schemes result from γ-γ coincidence relations and γ-ray intensities. Spin and parity assignments are based on DCO ratios of the γ rays as well as on deexcitation modes and lifetimes.

A. The level scheme of ^{82}Rb

The level scheme of ^{82}Rb deduced from the present work is shown in Fig. 4. It is in most parts consistent with previous work [31,32]. We extended the positive-parity sequences by tentative (15^+), (16^+), and (17^+) states at 4530.2, 5589.5, and 6011.7 keV, respectively. Based on the DCO ratio of the 1041.7 keV transition we assigned spin $J = 9$ to the 1732.1 keV level. The assignment of $J = 11$ for the 2616.3 keV level was deduced from the DCO ratios of the 393.9, 759.5, and 773.1 keV transitions and is consistent with the DCO ratios of the 839.5 and 913.5 keV transitions linking this level with positive-parity states. We consider multipolarity $M2$ unlikely for the 773.1, 884.8, and 1041.7 keV transitions, because the usual $M2$ transition strengths known in this mass region [33] correspond to lifetimes of $\tau \approx 100$ ns or more. Consequently, we assigned negative parity to the 1732.1 and 2616.3 keV levels, respectively. The spin assignments for the levels of the $M1$ band at 3026.9, 3499.9, 4047.5, and 4715.8 keV are based on the DCO ratios of the intraband $M1$ transitions. In addition to previous work [32] we observed crossover transitions at 883.5, 1019.2, 1215.8, and 1436.2 keV and found a further state at 5484.6 keV. Since our lifetime measurements (see Table III) exclude multipolarity $M2$ for

TABLE II. γ rays assigned to ^{84}Rb.

E_γ [a] (keV)	I_γ [b]	R_{DCO} [c]	E_γ^{gate} [d] (keV)	$\sigma\lambda$ [e]	J_i^π [f]	J_f^π [g]	E_i [h] (keV)
29.2(9)				$(M1)$ [i]	$6^{(+)}$	$5^{(+)}$	572.8
46.6(9)				$(M1)$ [i]	$7^{(+)}$	$6^{(+)}$	619.7
70.7(2)	299(37)			$(E1)$ [i]	$5^{(+)}$	$4^{(-)}$	543.3
76.4(2)	123(28)			$(E1)$ [i]	$5^{(+)}$	5^-	543.3
79.8(1)				$(E1)$ [i]	$5^{(+)}$	6^-	543.3
83.1(1)	169(27)			$(M1)$ [i]	$8^{(+)}$	$7^{(+)}$	702.9
135.5(2)	2.2(2)				$10^{(-)}$	(9^-)	3107.9
185.5(1)	44(2)	1.0(1)	83/631	$(M1)$	$11^{(-)}$	$10^{(-)}$	3122.1
214.4(1)	39(7)				$7^{(-)}$	6^-	678.1
218.3(2)	6.2(6)			$E2$ [i]	5^-	3^-	466.4
224.3(1)	21(1)			$E2$ [i]	$4^{(-)}$	3^-	472.3
225.0(1)	20(1)				$13^{(-)}$	$12^{(-)}$	3786.2
247.5(1)	74(7) [j]				3^-	2^-	247.5
286.8(2)	7.5(6)	0.9(1)	327	$(M1)$	$11^{(-)}$	$10^{(-)}$	3394.8
326.6(1)	28(2)	1.0(1)	83/631	$(M1)$	$12^{(-)}$	$11^{(-)}$	3721.5
344.9(2)	6.0(4)				$13^{(-)}$	$13^{(-)}$	4131.0
366.6(2)	7.1(6)	1.1(2)	327	$(M1)$	$11^{(-)}$	$10^{(-)}$	3394.8
401.3(5)	2.1(4)				(10^-)	(9^-)	2469.3
411.4(1)	18.4(9)	0.96(9)	83/631	$(M1)$	$11^{(-)}$	$10^{(-)}$	3122.1
424.4(1)	58(3)	0.86(5)	83	$M1$	$10^{(+)}$	$9^{(+)}$	1758.0
439.1(1)	34(2)	0.9(1)	186	$(M1)$	$12^{(-)}$	$11^{(-)}$	3561.2
445.1(1)	43(2)	1.1(1)	83/631	$M1$	$13^{(-)}$	$12^{(-)}$	4166.7
450.3(2)	23(1)	1.2(2)	186	$M1$	$13^{(-)}$	$12^{(-)}$	4131.0
453.1(1)	30(2)	1.0(1)	186	$M1$	$15^{(-)}$	$14^{(-)}$	5254.6
474.9(2)	6.9(4)	0.9(1)	186	$(M1)$	$10^{(-)}$	$9^{(-)}$	2936.8
489.3(2)	16.9(11)				(11^+)	$10^{(+)}$	2917.9
490.4(2)	23(2)				(12^+)	(11^+)	3408.2
538.4(2)	17.3(9)	0.9(2)	186	$M1$	$17^{(-)}$	$16^{(-)}$	6471.8
548.0(1)	34(2)	1.0(1)	83/631	$M1$	$14^{(-)}$	$13^{(-)}$	4714.7
557.1(5)	8.6(9)				$10^{(+)}$	(9^+)	2428.8
558.9(2)	37(2)	1.1(1)	186	$(M1)$	$12^{(-)}$	$11^{(-)}$	3680.9
569.7(2)	15.8(9)	1.0(2)	186	$(M1)$	$13^{(-)}$	$12^{(-)}$	4131.0
599.8(2)	23(1)	1.0(1)	186	$(M1)$	$12^{(-)}$	$11^{(-)}$	3721.5
618.7(3)	21(1)				$13^{(-)}$	$12^{(+)}$	3786.2
630.9(1)	100(5)	0.82(4)	83	$M1/E2$	$9^{(+)}$	$8^{(+)}$	1333.7
656.9(2)	17.1(11)	1.1(1)	83/631	$M1$	$15^{(-)}$	$14^{(-)}$	5371.9
670.6(2)	33(2)	1.2(2)	186	$M1$	$14^{(-)}$	$13^{(-)}$	4801.5
678.8(2)	22(1)	1.2(2)	186	$M1$	$16^{(-)}$	$15^{(-)}$	5933.4
690.5(3)	18.8(11)	0.9(1)	83/631	$M1$	$12^{(+)}$	$11^{(+)}$	3167.1
718.8(2)	38(2)	1.0(1)	83/631	$M1$	$11^{(+)}$	$10^{(+)}$	2476.7
719.7(3)	7.5(9)	1.1(2)	186	$(M1)$	$8^{(-)}$	$7^{(-)}$	1397.9
722.6(4)	15.0(11)				(16^-)	$15^{(-)}$	6094.8
766.4(5)	8.4(8)				(17^-)	(16^-)	6861.1
771.3(12)	4.7(8)				$13^{(-)}$	$11^{(-)}$	4166.7
838.2(3)	20(1)					(12^+)	4246.4
868.0(14)	1.9(2)				$10^{(-)}$	(9^-)	2936.8
911.0(3)	10.7(6)	1.2(3)	186	$(M1)$	(18^-)	$17^{(-)}$	7382.8
959.0(3)	11.1(9)				(8^-)	$8^{(+)}$	1662.4
984.8(5)	6.4(6)				(8^-)	$7^{(-)}$	1662.4
994.8(5)	14.6(11)				$14^{(-)}$	$12^{(-)}$	4714.7
1015.2(3)	21(1)	1.0(2)	186	$(M1)$	$14^{(-)}$	$13^{(-)}$	4801.5

TABLE II. (*Continued*).

E_γ[a] (keV)	I_γ[b]	R_{DCO}[c]	E_γ^{gate}[d] (keV)	$\sigma\lambda$[e]	J_i^π[f]	J_f^π[g]	E_i[h] (keV)
1054.9(2)	63(3)	1.6(1)	83	$E2$	$10^{(+)}$	$8^{(+)}$	1758.0
1063.8(3)	7.9(8)	0.8(1)	186	$(M1)$	$9^{(-)}$	$8^{(-)}$	2461.8
1095.3(2)	58(3)	0.89(9)	83/631	$(M1)$	$10^{(+)}$	$9^{(+)}$	2428.8
1158.2(8)	5.3(6)				(11^+)	$10^{(+)}$	2917.9
1169.0(6)	12.4(11)				(9^+)	$8^{(+)}$	1871.7
1181.0(3)	9.0(6)				$10^{(-)}$	$10^{(+)}$	2936.8
1205.4(5)	13.9(9)				$15^{(-)}$	$13^{(-)}$	5371.9
1227.1(12)	1.7(4)				(9^-)	(7^-)	2972.3
1239.1(8)	6.2(6)				$14^{(-)}$	$12^{(-)}$	4801.5
1252.6(11)	3.4(4)				$12^{(-)}$	(10^-)	3721.5
1274.0(4)	6.9(6)				$10^{(-)}$	(8^-)	2936.8
1278.2(13)	2.1(6)				(7^-)	5^-	1744.9
1365.4(5)	10.1(9)				$10^{(-)}$	(8^-)	3028.1
1376.5(3)	22(1)	0.86(9)	83/631	$(E1)$	$10^{(-)}$	$9^{(+)}$	2710.6
1380.7(5)	13.5(9)				(16^-)	$14^{(-)}$	6094.8
1390.0(5)	11.1(8)				(9^-)	$7^{(-)}$	2068.1
1408.8(2)	50(3)	1.6(1)	83/631	$E2$	$12^{(+)}$	$10^{(+)}$	3167.1
1445.5(15)	2.8(4)				$10^{(-)}$	(8^-)	3107.9
1489.3(9)	7.5(8)				(17^-)	$15^{(-)}$	6861.1
1636.4(4)	9.9(8)	1.0(2)	83/631	$(E1)$	$11^{(-)}$	$10^{(+)}$	3394.8
1649.8(6)	12.2(8)				(12^+)	$10^{(+)}$	3408.2
1657.7(5)	14.6(11)	1.0(3)	1055/1409	$E2$	$14^{(+)}$	$12^{(+)}$	4824.7
1771.9(9)	4.5(4)				$10^{(-)}$	$9^{(+)}$	3107.9

[a]Transition energy. The error in parentheses is given in units of the last digit.
[b]Relative intensity of the γ ray normalized to $I_\gamma = 100$ of the $9^{(+)} \rightarrow 8^{(+)}$ transition at 630.9 keV.
[c]DCO ratio $R_{DCO} = W(90°,35°/145°)/W(35°/145°,90°)$.
[d]Energy of the gating transition used for the determination of the DCO ratio.
[e]Multipolarity compatible with the DCO ratio, the deexcitation mode, and the lifetime of the initial state.
[f]Spin and parity of the initial state.
[g]Spin and parity of the final state.
[h]Energy of the initial state.
[i]Taken from Ref. [34].
[j]Coincidence intensity observed via the 218.3 keV transition. Feeding from the 6^- isomeric state at 463.7 keV ($\tau = 29.6$ min) has not been observed in the present coincidence experiment.

the crossover transitions, we assigned negative parity to all states of the $M1$ band in agreement with the tentative assignment given in Ref. [32].

B. The level scheme of ^{84}Rb

The level scheme of ^{84}Rb deduced from the present work is shown in Fig. 5. Levels in ^{84}Rb have been known from previous work up to 5^-, (7^-), and (10^+) states at 466.4, 678.1, and 1758.0 keV only [34]. We extended the likely positive-parity sequence up to a $14^{(+)}$ state at 4824.7 keV. The spin assignments made for the states of this sequence are based on DCO ratios of intraband transitions. We found a new level sequence feeding positive-parity states with levels at 1871.7, 2428.8, 2917.9, 3408.2, and 4246.4 keV. However, tentative spin and parity assignments could be made for some of these levels only. We established four new level sequences of probably negative parity: On top of the previously known 5^- state at 466.4 keV we found levels at 1744.9, 2972.3, and 3107.9 keV, and assigned spins and parities of (7^-), (9^-), and $10^{(-)}$, respectively, to these states. The assignment of $J = 10$ for the 3107.9 keV level is based on DCO ratios of populating transitions. We observed a level sequence including $8^{(-)}$ to $13^{(-)}$ states at energies of 1397.9, 2461.8, 2936.8, 3122.1, 3561.2, and 3786.2 keV built on the previously known $7^{(-)}$ state. Moreover, we observed two $\Delta J = 1$ sequences on top of these sequences. One sequence includes levels at 3394.8, 3721.5, 4166.7, 4714.7, 5371.9, 6094.8, and 6861.1 keV. The spin assignments for these levels are based on the DCO ratios of the 599.8 and 1636.4 keV γ rays and the intraband transitions. The intraband $\Delta J = 1$ transitions are considered as $M1$ transitions on the basis of the short lifetimes of the emitting states (see Table IV) and of the observation of $\Delta J = 2$ crossover transitions. The other sequence comprises levels at 3680.9, 4131.0, 4801.5, 5254.6, 5933.4, 6471.8, and 7382.8 keV. The spin assignments are based on the DCO ratios of the transitions within the se-

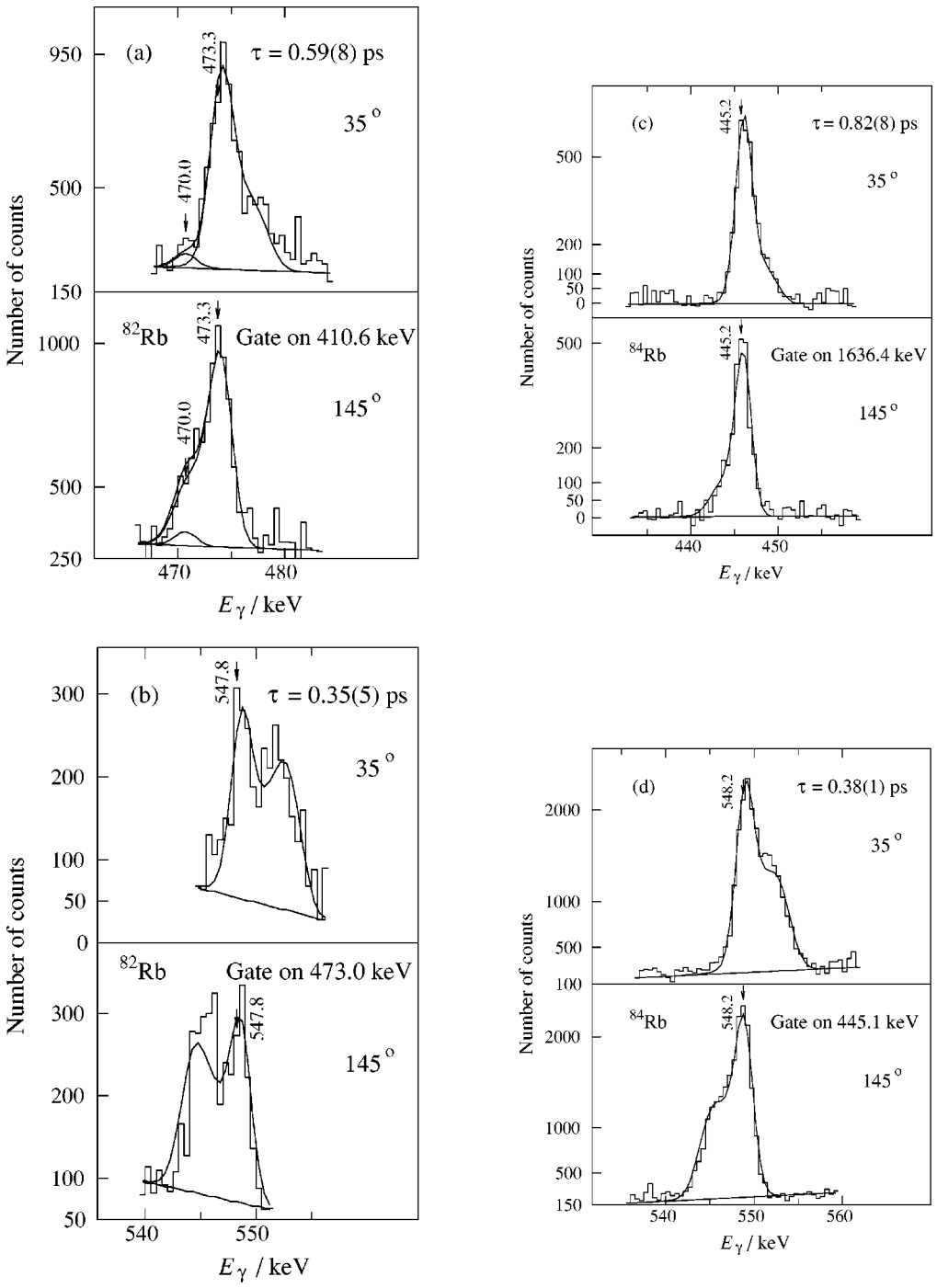

FIG. 3. Examples of the line-shape analysis using the DSA method. Mean lifetimes were deduced from simultaneous fits of calculated to experimental line shapes at the complementary observation angles of 35° and 145°. Feeding corrections are included. The values of energies, lifetimes, and their errors are results of the presented fits. The three curves in panel (a) are the calculated line shapes for the two peaks and the total.

quence. We tentatively assign negative parity to both the $\Delta J = 1$ sequences.

After our preceding short publication [19] an in-beam study of ^{84}Rb using the ^{70}Zn(^{18}O,$p3n$) reaction [35] was published. The level scheme presented in that work contains the main structures discussed here. Some of the transitions linking the 5^- to $10^{(-)}$ states were proposed in a different order or with different energies, which are not consistent with the present experiment. Furthermore, the levels of the sequence above the 3680.9 keV state were arranged into two sequences with a few additional transitions, which we cannot confirm.

IV. TAC-MODEL CALCULATIONS

In order to compare the absolute experimental transition strengths within the $M1$ bands of ^{82}Rb and ^{84}Rb with the

TABLE III. Mean lifetimes of states in ^{82}Rb.

E_i (keV)[a]	E_γ (keV)[b]	τ (ps)[c]
863	562.6	0.28(8)
1281	980.0	0.98(8)
1902	620.7	<0.55[d]
2551	1270.1	<0.9[d]
3027	410.6	0.58(13)
3500	473.0	0.59(11)
4048	547.7	0.35(7)
4716	668.4	<1[d]

[a]Level energy.
[b]Energy of the γ ray used for the line-shape analysis in connection with the DSA method.
[c]Adopted level lifetime. The error in parentheses includes the statistical error, uncertainties of feeding times and feeding intensities. Uncertainties of the nuclear and electronic stopping power, which may be in the order of 10%, are not included.
[d]Upper limit deduced from the effective lifetime without feeding correction.

predictions of the TAC model we performed calculations described in detail in our preceding short publication [19]. Those calculations were based on the lowest-lying $4qp$ configuration for $Z=37$ and $N=45$, 47, which is $\pi(fp)\ \ \pi(g_{9/2}^2)\ \nu(g_{9/2})$. We obtained equilibrium deformations of $\epsilon_2=0.16$ and $\epsilon_2=0.14$ for ^{82}Rb and ^{84}Rb, respectively. Furthermore, both nuclei turned out to be soft with respect to γ deformation. The potential-energy curves are asymmetric, tending to

TABLE IV. Mean lifetimes of states in ^{84}Rb.

E_i (keV)[a]	E_γ (keV)[b]	τ (ps)[c]
1334	630.9	0.85(15)
1758	424.4	1.6(2)
2477	718.8	0.28(3)
3167	690.5	<1.2[d]
4167	445.1	0.82(12)
4715	548.0	0.38(3)
5372	656.9/1205.4	0.25(4)
6095	722.6/1380.7	0.16(4)
6861	766.4/1489.3	<0.45[d]
4131	450.3	0.41(7)
4802	670.6	0.07(2)
5255	453.1	0.63(9)
5933	678.8	0.11(2)
6472	538.4	<0.52[d]

[a]Level energy.
[b]Energy of the γ ray used for the line-shape analysis in connection with the DSA method.
[c]Adopted level lifetime. The error in parentheses includes the statistical error, uncertainties of feeding times and feeding intensities. Uncertainties of the nuclear and electronic stopping power, which may be in the order of 10%, are not included.
[d]Upper limit deduced from the effective lifetime without feeding correction.

TABLE V. Experimental transition strengths in ^{82}Rb.

E_γ[a] (keV)	J_i^π	J_f^π	$B(M1)$ (μ_N^2)	$B(E2)$ (e^2 fm^4)
562.6	$9^{(+)}$	$8^{(+)}$	$1.13^{+0.45}_{-0.25}$	
417.8	$10^{(+)}$	$9^{(+)}$	$0.17^{+0.03}_{-0.03}$	
980.0	$10^{(+)}$	$8^{(+)}$		729^{+83}_{-71}
620.7	$11^{(+)}$	$10^{(+)}$	>0.35	
1038.2	$11^{(+)}$	$9^{(+)}$		>197
1270.1	$12^{(+)}$	$10^{(+)}$		>275
318.3	12^-	(11^-)	$0.36^{+0.15}_{-0.10}$	
410.6	12^-	11^-	$1.24^{+0.37}_{-0.24}$	
473.0	13^-	12^-	$0.77^{+0.20}_{-0.13}$	
883.5	13^-	11^-		384^{+154}_{-106}
547.7	14^-	13^-	$0.74^{+0.22}_{-0.14}$	
1019.2	14^-	12^-		511^{+193}_{-129}
668.4	15^-	14^-	>0.11	
1215.8	15^-	13^-		>110

[a]$\Delta J=1$ transitions are considered as pure $M1$ transitions. Possible $E2$ admixtures to transitions of mixed or unknown multipole order are neglected (see Table I).

positive γ values for ^{82}Rb and negative γ values for ^{84}Rb. We adopted values of $\gamma=20°$ and $\gamma=-15°$ for ^{82}Rb and ^{84}Rb, respectively. The given deformation parameters ϵ_2 and γ were used throughout the considered frequency range. We presented absolute transition strengths resulting from these calculations already in Ref. [19], whereas experimental values were not available at that time. This implies that the parameters used in the calculations were not optimized to reproduce the absolute experimental transition strengths presented here for the first time. Experimental transition strengths derived from the present experiment (see Tables V and VI) are compared with the values predicted by the TAC-model calculations described above in Figs. 6, 7, 8, and 9, respectively. The calculated values were taken from Table I in the short publication [19].

The experimental $B(M1)$ values in ^{82}Rb (see Fig. 6) tend to decrease with increasing rotational frequency. This behavior is similar to the calculated one indicating the shears mechanism. However, the calculated values are by some 20 to 30 % smaller than the experimental ones. The slope of the calculated $B(M1)$ curve correlates with the tilt angle which increases from about 68° at $\hbar\omega=0.3$ MeV to about 73° at $\hbar\omega=0.6$ MeV, but changes only slightly at higher frequencies, reaching about 76° at $\hbar\omega=0.77$ MeV. The experimental $B(E2)$ values (see Fig. 7) may increase slightly with increasing frequency as is predicted in the calculations. Furthermore, the order of magnitude of the experimental values is reproduced by the calculation, which reflects that the calculated equilibrium deformation of $\epsilon_2=0.16$ (see Ref. [19]) is realistic.

The experimental $B(M1)$ values in ^{84}Rb (see Fig. 8) decrease slightly up to $\hbar\omega\approx0.65$ MeV, but may increase to higher frequency. The calculated decrease is more pronounced than the experimental one. As in ^{82}Rb, the slope of the calculated $B(M1)$ curve correlates with the behavior of

TABLE VI. Experimental transition strengths in ^{84}Rb.

E_γ[a] (keV)	J_i^π	J_f^π	$B(M1)$ (μ_N^2)	$B(E2)$ (e^2 fm^4)
630.9	$9^{(+)}$	$8^{(+)}$	$0.26^{+0.06}_{-0.04}$	
424.4	$10^{(+)}$	$9^{(+)}$	$0.22^{+0.05}_{-0.03}$	
1054.9	$10^{(+)}$	$8^{(+)}$		204^{+40}_{-32}
718.8	$11^{(+)}$	$10^{(+)}$	$0.54^{+0.06}_{-0.05}$	
690.5	$12^{(+)}$	$11^{(+)}$	>0.03	
1408.8	$12^{(+)}$	$10^{(+)}$		>87
445.1	$13^{(-)}$	$12^{(-)}$	$0.70^{+0.14}_{-0.10}$	
771.3	$13^{(-)}$	$11^{(-)}$		357^{+69}_{-52}
548.0	$14^{(-)}$	$13^{(-)}$	$0.63^{+0.08}_{-0.07}$	
994.8	$14^{(-)}$	$12^{(-)}$		670^{+125}_{-106}
656.9	$15^{(-)}$	$14^{(-)}$	$0.44^{+0.11}_{-0.08}$	
1205.4	$15^{(-)}$	$13^{(-)}$		576^{+160}_{-115}
722.6	(16^-)	$15^{(-)}$	$0.49^{+0.21}_{-0.12}$	
1380.7	(16^-)	$14^{(-)}$		482^{+210}_{-125}
766.4	(17^-)	(16^-)	>0.13	
1489.3	(17^-)	$15^{(-)}$		>105
344.9	$13^{(-)}$	$13^{(-)}$	$0.44^{+0.15}_{-0.10}$	
450.3	$13^{(-)}$	$12^{(-)}$	$0.78^{+0.21}_{-0.15}$	
569.7	$13^{(-)}$	$12^{(-)}$	$0.26^{+0.08}_{-0.06}$	
670.6	$14^{(-)}$	$13^{(-)}$	$1.45^{+0.70}_{-0.38}$	
1015.2	$14^{(-)}$	$13^{(-)}$	$0.27^{+0.14}_{-0.08}$	
1239.1	$14^{(-)}$	$12^{(-)}$		411^{+240}_{-133}
453.1	$15^{(-)}$	$14^{(-)}$	$0.96^{+0.16}_{-0.12}$	
678.8	$16^{(-)}$	$15^{(-)}$	$1.64^{+0.36}_{-0.25}$	
538.4	$17^{(-)}$	$16^{(-)}$	>0.69	

[a]$\Delta J=1$ transitions are considered as pure $M1$ transitions. Possible $E2$ admixtures to transitions of mixed or unknown multipole order are neglected (see Table II).

the tilt angle which increases from about 62° at $\hbar\omega=0.3$ MeV to about 72° at $\hbar\omega=0.6$ MeV and then to 75° at $\hbar\omega=0.74$ MeV. The possible increase of the experimental $B(M1)$ values around $\hbar\omega\approx0.7$ MeV is not described by the calculations. This increase may indicate a change of the structure including a loss of collectivity as shown by the decreasing $B(E2)$ values around $\hbar\omega\approx0.7$ MeV (see Fig. 9). Also for ^{84}Rb, the calculated equilibrium deformation of $\epsilon_2=0.14$ (see Ref. [19]) turns out to be realistic.

V. SHELL-MODEL CALCULATIONS FOR ^{84}Rb

The nuclide ^{84}Rb has 37 protons and 47 neutrons, i.e., three neutron holes in the $N=50$ shell, and is accessible to shell-model calculations. Therefore, we interpreted the structure of ^{84}Rb in the framework of the shell model which may give an alternative description of the phenomena discussed in Sec. IV. The calculations were carried out with the code RITSSCHIL [36].

The model space used in our calculations includes the active proton orbitals $\pi(0f_{5/2},1p_{3/2},1p_{1/2},0g_{9/2})$ and neutron orbitals $\nu(1p_{1/2},0g_{9/2})$ relative to a hypothetic ^{66}Ni core. Since an empirical set of effective interactions for this model space is not available up to now, various empirical interactions have been combined with results of schematic nuclear interactions applying the surface delta interaction. Details of this procedure are described in our previous shell-model studies of nuclei with $N=48$ [37,38], $N=49$ [39,40], $N=50$ [39,41–44], $N=51$, 52 [45], and $N=53$, 54 [46].

The single-particle energies relative to the ^{66}Ni core have been derived from the single-particle energies of the proton orbitals given in Ref. [47] with respect to the ^{78}Ni core and from the neutron single-hole energies of the $1p_{1/2},0g_{9/2}$ orbitals [48]. The transformation of these single-particle ener-

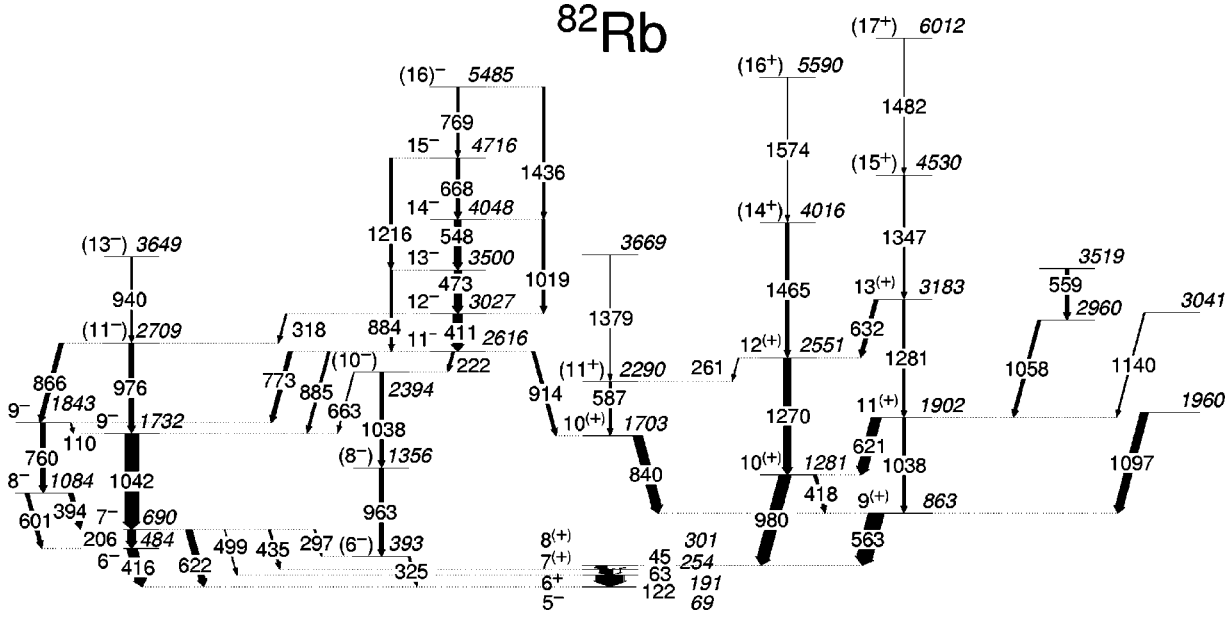

FIG. 4. Level scheme of ^{82}Rb deduced from the present experiments.

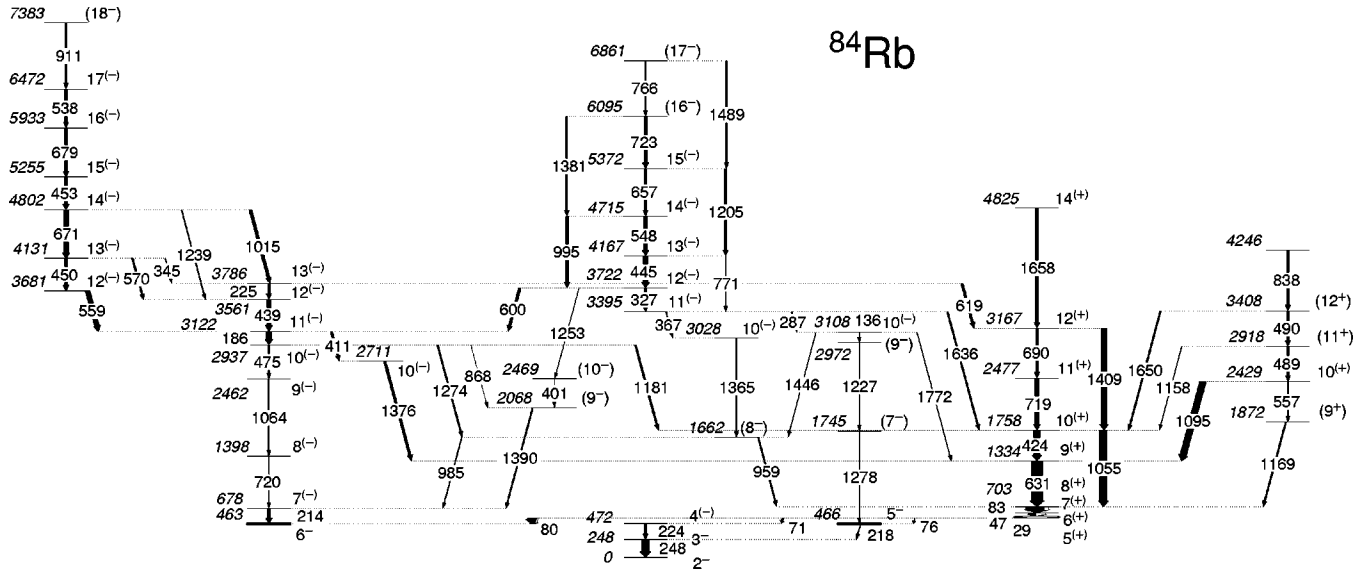

FIG. 5. Level scheme of ^{84}Rb deduced from the present experiments.

gies to those relative to the ^{66}Ni core has been performed [49] on the basis of the effective residual interactions given in, e.g., Refs. [39,40]. The obtained values are $\epsilon^{\pi}_{f_{5/2}} = -9.106$ MeV, $\epsilon^{\pi}_{p_{3/2}} = -9.033$ MeV, $\epsilon^{\pi}_{p_{1/2}} = -4.715$ MeV, $\epsilon^{\pi}_{g_{9/2}} = -0.346$ MeV, $\epsilon^{\nu}_{p_{1/2}} = -7.834$ MeV, and $\epsilon^{\nu}_{g_{9/2}} = -6.749$ MeV. These single-particle energies and the corresponding values for the strengths of the residual interactions have been used to calculate level energies as well as $M1$ and $E2$ transition strengths. For the latter, effective g factors of $g_s^{\rm eff} = 0.7 g_s^{\rm free}$ and effective charges of $e_\pi = 1.72e$, $e_\nu = 1.44e$ [50], respectively, have been applied.

The nucleus ^{84}Rb has nine protons and nine neutrons in the considered configuration space. To make the calculations feasible a truncation of the occupation numbers was applied. At most three protons are allowed to be lifted to the $(1p_{1/2}, 0g_{9/2})$ subshell. Two of the neutrons occupy the $1p_{1/2}$ orbital and seven the $0g_{9/2}$ orbital. With these restrictions configuration spaces with dimensions smaller than 19 600 were obtained.

A. Results for low-lying states

Calculated level energies are compared with experimental ones in Fig. 10. The experimental positive-parity states are well reproduced up to $J = 12$. The order of the very close-lying 5^+, 6^+, 7^+, and 8^+ states is, however, not exactly reproduced. The 5^+ to 9^+ states are characterized by the configuration $\pi(0g^1_{9/2})\nu(0g^{-3}_{9/2})_{J_\nu}$ with $J_\nu = 7/2$ or $9/2$ while in the main components of the lowest-lying 10^+ to 15^+

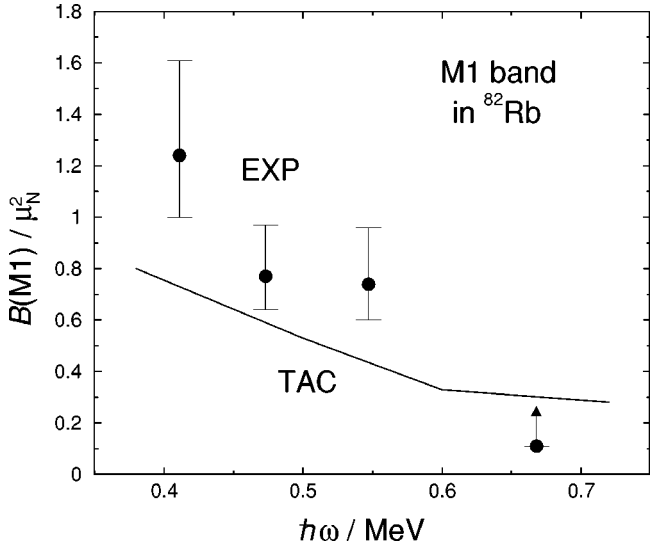

FIG. 6. Experimental and calculated $M1$ transition strengths in the negative-parity $M1$ band of ^{82}Rb. The solid line connects the $B(M1)$ values calculated at particular values of $\hbar\omega$ and is therefore not a smooth curve.

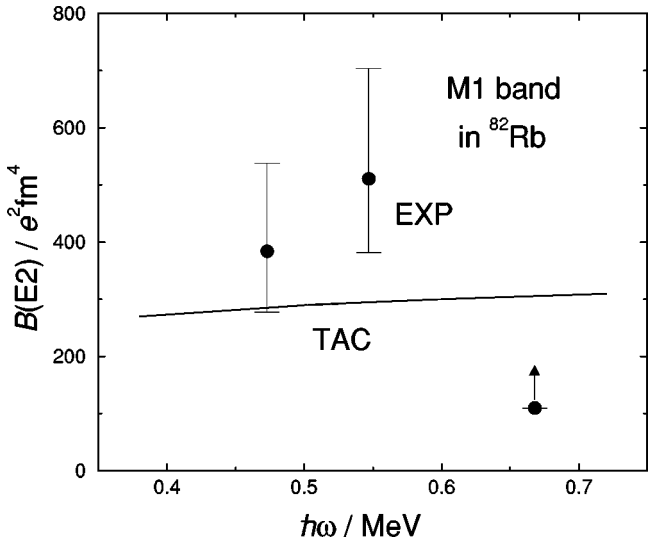

FIG. 7. Experimental and calculated $E2$ transition strengths in the negative-parity $M1$ band of ^{82}Rb.

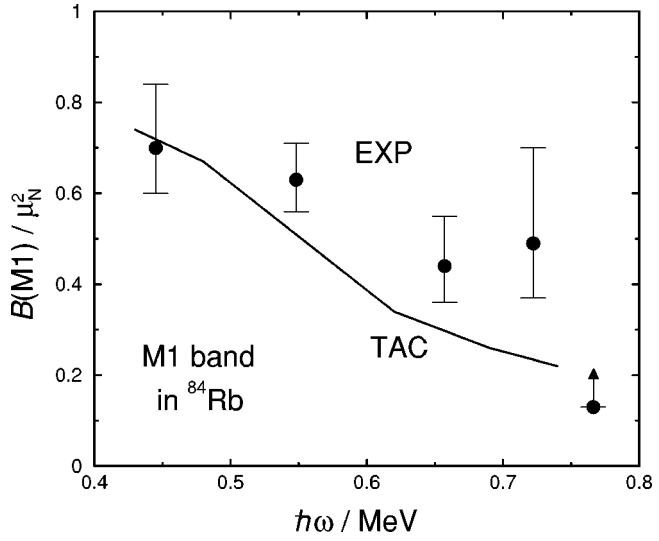

FIG. 8. Experimental and calculated $M1$ transition strengths in the negative-parity $M1$ band of ^{84}Rb. The solid line connects the $B(M1)$ values calculated at particular values of $\hbar\omega$ and is therefore not a smooth curve.

states the neutrons couple to $J_\nu = 13/2$, 17/2, or 21/2. The second states with $J^\pi = 10^+$, 11^+, and 12^+ are dominated by the configuration $\pi(0f_{5/2}^{-1}1p_{3/2}^{-1}0g_{9/2}^{1})\nu(0g_{9/2}^{-3})$. The calculated 13^+ and 14^+ states lie below the experimental ones in contrast to the states with smaller spin. This may indicate that the structures of these states differ from the single-particle configurations discussed here.

Calculated and experimental transition strengths between positive-parity states are compared in Table VII. The calculated $B(M1,9^+ \rightarrow 8^+)$, $B(M1,11^+ \rightarrow 10^+)$, and $B(E2,10^+ \rightarrow 8^+)$ values exceed the experimental ones by factors of two to four, while the $B(M1,10^+ \rightarrow 9^+)$ value is predicted by a factor of 10 too small in the calculation.

The calculated lowest-lying negative-parity states describe roughly the experimental ones (see Fig. 10). However,

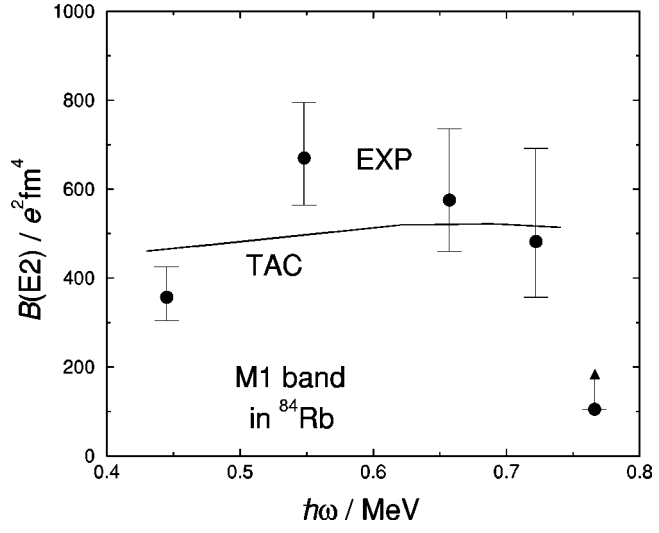

FIG. 9. Experimental and calculated $E2$ transition strengths in the negative-parity $M1$ band of ^{84}Rb.

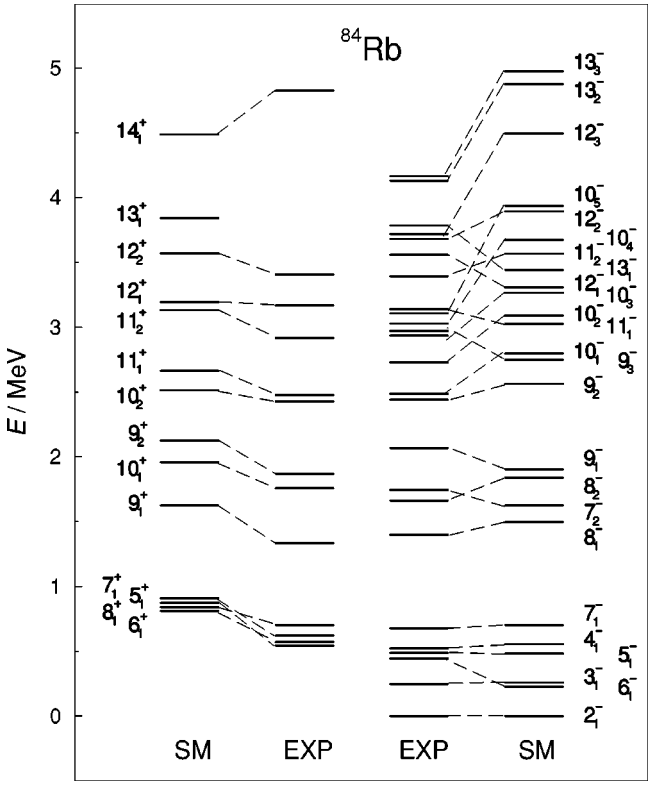

FIG. 10. Comparison of experimental with calculated level energies in ^{84}Rb.

the order of close-lying calculated states differs in some cases from the experiment, especially for states of higher order with $J \geqslant 10$. The 2^- ground state is described by the configuration $\pi(0f_{5/2}^{-1})\nu(0g_{9/2}^{-3})_{J_\nu}$ with $J_\nu = 7/2$ and 9/2. These are also the main configurations of the 6_1^- and 7_1^- states while the 3_1^-, 4_1^-, and 5_1^- states are dominated by the configuration $\pi(1p_{3/2}^{-1})\nu(0g_{9/2}^{-3})_{J_\nu}$. The 8_1^- and 9_1^- states have the main configuration $\pi(0f_{5/2}^{-1}1p_{3/2}^{-1}1p_{1/2}^{1})\nu(0g_{9/2}^{-3})_{J_\nu}$, i.e., a proton pair is broken where one proton is lifted to the $1p_{1/2}$ orbital. The 10_1^- to 13_1^- states, however, are generated by recoupling the spins of the $0g_{9/2}$ neutron holes instead of breaking proton pairs. Thus, they are dominated by configurations analogous to those of the 2_1^- to 7_1^- states (see above), but with $J_\nu = 17/2$ or 21/2. The configurations discussed above also predominate with varying partitions in the negative-parity states of higher order. However, for $J \geqslant 11$ also excitations of two protons from the $1p_{3/2}$ and $0f_{5/2}$ or-

TABLE VII. Experimental and calculated transition strengths between positive-parity states ^{84}Rb.

J_i^π	J_f^π	$B(M1)_{\rm exp}$ (μ_N^2)	$B(M1)_{\rm SM}$ (μ_N^2)	$B(E2)_{\rm exp}$ (e^2 fm^4)	$B(E2)_{\rm SM}$ (e^2 fm^4)
9_1^+	8_1^+	$0.26^{+0.06}_{-0.04}$	1.07		
10_1^+	9_1^+	$0.22^{+0.05}_{-0.03}$	0.05		
10_1^+	8_1^+			204^{+40}_{-32}	386
11_1^+	10_1^+	$0.54^{+0.06}_{-0.05}$	0.98		

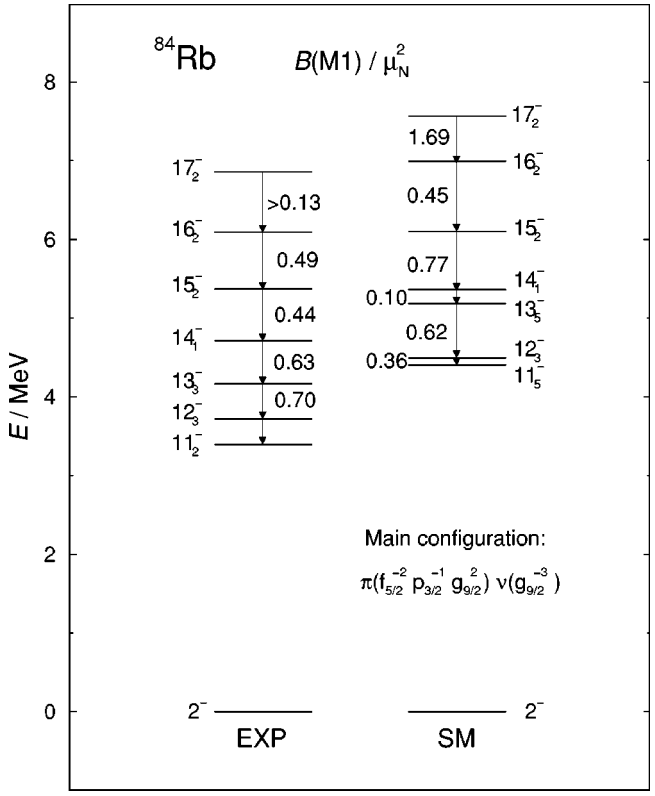

FIG. 11. Comparison of experimental with calculated level energies and $B(M1)$ transition strengths in the negative-parity $M1$ band in ^{84}Rb.

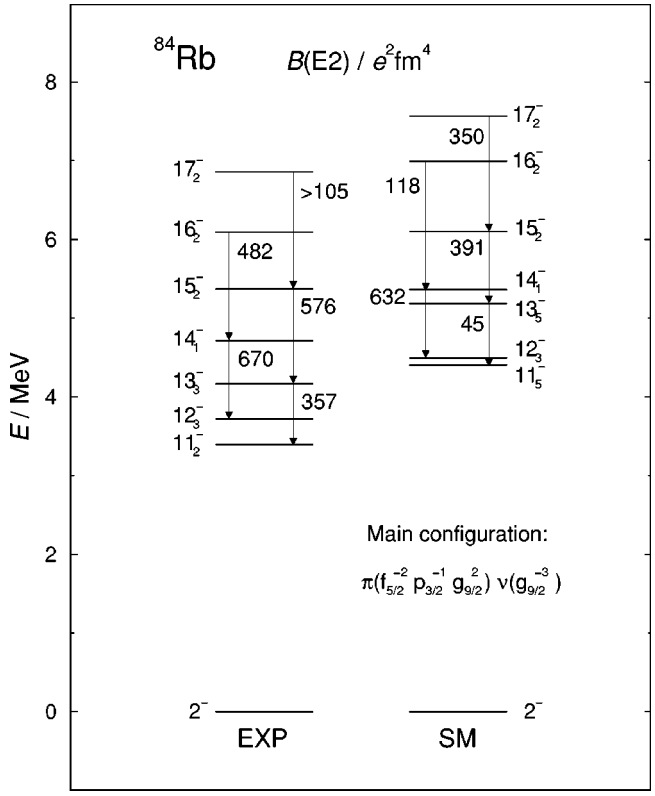

FIG. 12. Comparison of experimental with calculated level energies and $B(E2)$ transition strengths in the negative-parity $M1$ band in ^{84}Rb.

bitals to the $0g_{9/2}$ orbital contribute considerably to the wave functions of certain states (see Sec. V B).

B. Results for the $M1$ sequences

An interesting question is whether the shell-model calculations can describe the regular $M1$ band discussed in Sec. IV. Because there are several closely lying experimental as well as calculated states of a given spin, especially for $J^\pi = 11^-$, 12^-, and 13^-, the combination of states with similar properties may be more suitable than a formal assignment of the first calculated state to the lowest-lying experimental one of a given spin, and so on. Therefore, we combined the lowest states linked by transitions with $B(M1)$ values in the order of the experimental ones ($B(M1) \geqslant 0.1\mu_N^2$), which results in the sequence $11_5^- - 12_3^- - 13_5^- - 14_1^- - 15_2^- - 16_2^- - 17_2^-$. It turns out that all these states have the main configuration $\pi(0f_{5/2}^{-2}1p_{3/2}^{-1}0g_{9/2}^2)\nu(0g_{9/2}^{-3})$. It is remarkable, that this configuration corresponds to the $4qp$ configuration adopted in the TAC-model calculations for the $M1$ band (see Sec. IV). This correspondence demonstrates that the coupling of the spin vectors of protons and neutrons in the high-j $0g_{9/2}$ orbitals is the basic mechanism for generating level sequences linked by $M1$ transitions with large transition strengths. Level energies, $M1$ and $E2$ transition strengths calculated for the obtained level sequence are compared with experimental ones in Figs. 11 and 12, respectively. This comparison shows that the calculations predict roughly the energy range of the experimental $M1$ band as well as the order of magnitude of the $B(M1)$ and $B(E2)$ values. However, the calculated level sequence does not reproduce the bandlike properties such as the regularity ($J \sim E_\gamma^{M1}$) or the steady decrease of the $B(M1)$ values with increasing spin, i.e., this sequence does not describe a shears-type band. This may indicate that the truncation of the model space excludes orbitals that are important for generating regular level sequences and/or that particular residual-interaction matrix elements are not realistic. In a shell-model study of shears bands in light Pb nuclei it was found that regular bands are created, if several high-j protons and high-j neutron holes interact with many low-spin fp orbitals [51]. If one applies this to ^{84}Rb, then the number of proton particle-hole excitations of the type $\pi[(0f_{5/2}1p_{3/2})^{-m-1}(1p_{1/2}0g_{9/2})^m]$ should be such that the number of particles in the fp shell is in the middle of the shell ($m \approx 4$ to 6). However, in the present calculations this number was limited to $m=3$ (see above).

Figure 13 compares level energies and $B(M1)$ values of the $M1$ sequence starting with the $12^{(-)}$ state at 3680.9 keV with calculated ones. In contrast to the $M1$ band discussed above, this sequence is not regular and $E2$ crossover transitions were not observed. Out of the calculated states, those states were combined that are connected by transitions with $B(M1)$ values approaching the order of the experimental ones but not already used for the $M1$ band discussed above. The calculated sequence lies again roughly in the same energy range as the experimental one. The order of magnitude

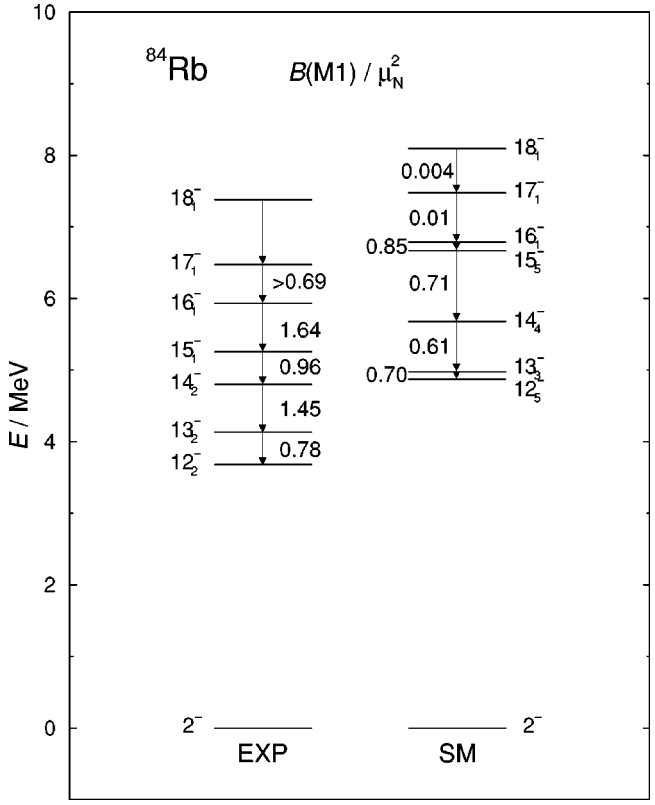

FIG. 13. Comparison of experimental with calculated level energies and $B(M1)$ transition strengths in the second negative-parity $M1$ sequence in ^{84}Rb.

of the $B(M1)$ values is reproduced for the lowest four transitions. The 12_5^-, 14_4^-, 15_5^-, 16_1^-, and 18_1^- states are dominated by the configuration $\pi(0f_{5/2}^{-2}1p_{3/2}^{-1}0g_{9/2}^2)\,\nu(0g_{9/2}^{-3})$ like the states of the $M1$ band while the 13_3^- and 17_1^- states include the main configurations $\pi(1p_{3/2}^{-2}1p_{1/2}^1)\,\nu(0g_{9/2}^{-3})$ and $\pi(0f_{5/2}^{-3}0g_{9/2}^2)\,\nu(0g_{9/2}^{-3})$, respectively.

VI. CONCLUSIONS

Excited states in the odd-odd nuclei $^{82}Rb_{45}$ and $^{84}Rb_{47}$ were studied with the spectrometer GASP. The regular $M1$ bands found in both nuclei display characteristics of magnetic rotation. These bands are well described in the TAC model on the basis of the lowest negative-parity $4qp$ configuration $\pi(fp)\ \pi(g_{9/2}^2)\ \nu(g_{9/2})$. The TAC calculations reproduce well the bandlike properties and, moreover, the absolute experimental $B(M1)$ and $B(E2)$ transition strengths in the $M1$ bands of both nuclei. This agreement confirms our former interpretation of the $M1$ bands in terms of magnetic rotation based on $B(M1)/B(E2)$ ratios [19,20].

In addition, excited states in ^{84}Rb were interpreted in terms of the shell model using the model space $\pi(0f_{5/2},1p_{3/2},1p_{1/2},0g_{9/2})\ \nu(1p_{1/2},0g_{9/2})$. These calculations reproduce the low-spin states. Calculated states with the main configuration $\pi(0f_{5/2}^{-2}1p_{3/2}^{-1}0g_{9/2}^2)\ \nu(0g_{9/2}^{-3})$ can be combined into an $M1$ sequence that roughly reproduces the energy range of the experimental states and the order of magnitude of the experimental transition strengths. However, the calculations in the present limited configuration space do not describe the features of magnetic rotation such as regular level spacings and $B(M1)$ values which decrease with increasing rotational frequency.

ACKNOWLEDGMENTS

This work was supported by the European Commission within the TMR/LSF program under Contract No. ERBFMGECT980110. G.R. and R.S. acknowledge financial support by NATO Grant No. PST.CLG.977744.

[1] B. Fant, R. J. Tanner, P. A. Butler, A. N. James, G. D. Jones, R. J. Poynter, C. A. White, K. L. Ying, D. J. G. Love, J. Simpson, and K. A. Connell, J. Phys. G **17**, 319 (1991).
[2] R. M. Clark, R. Wadsworth, E. S. Paul, C. W. Beausang, I. Ali, A. Astier, D. M. Cullen, P. J. Dagnall, P. Fallon, M. J. Joyce, M. Meyer, N. Redon, P. H. Regan, W. Nazarewicz, and R. Wyss, Phys. Lett. B **275**, 247 (1992).
[3] G. Baldsiefen, H. Hübel, D. Mehta, B. V. Thirumala Rao, U. Birkental, G. Fröhlingsdorf, M. Neffgen, N. Nenoff, S. C. Pancholi, N. Singh, W. Schmitz, K. Theine, P. Willsau, H. Grawe, J. Heese, H. Kluge, K. H. Maier, M. Schramm, R. Schubart, and H. J. Maier, Phys. Lett. B **275**, 252 (1992).
[4] A. Kuhnert, M. A. Stoyer, J. A. Becker, E. A. Henry, M. J. Brinkman, S. W. Yates, T. F. Wang, J. A. Cizewski, F. S. Stephens, M. A. Deleplanque, R. M. Diamond, A. O. Macchiavelli, J. E. Draper, F. Azaiez, W. H. Kelly, and W. Korten, Phys. Rev. C **46**, 133 (1992).
[5] R. M. Clark, R. Wadsworth, E. S. Paul, C. W. Beausang, I. Ali, A. Astier, D. M. Cullen, P. J. Dagnall, P. Fallon, M. J. Joyce, M. Meyer, N. Redon, P. H. Regan, J. F. Sharpey-Schafer, W. Nazarewicz, and R. Wyss, Nucl. Phys. **A562**, 121 (1993).
[6] G. Baldsiefen, H. Hübel, W. Korten, D. Mehta, N. Nenoff, B. V. Thirumala Rao, P. Willsau, H. Grawe, J. Heese, K. H. Maier, R. Schubart, S. Frauendorf, and H. J. Maier, Nucl. Phys. **A574**, 521 (1994).
[7] M. Neffgen, G. Baldsiefen, S. Frauendorf, H. Grawe, J. Heese, H. Hübel, H. Kluge, A. Korichi, W. Korten, K. H. Maier, D. Mehta, J. Meng, N. Nenoff, M. Piiparinen, M. Schönhofer, R. Schubart, U. J. van Severen, N. Singh, G. Sletten, B. V. Thirumala Rao, and P. Willsau, Nucl. Phys. **A595**, 499 (1995).
[8] R. M. Clark, S. J. Asztalos, G. Baldsiefen, J. A. Becker, L. Bernstein, M. A. Deleplanque, R. M. Diamond, P. Fallon, I. M. Hibbert, H. Hübel, R. Krücken, I. Y. Lee, A. O. Macchiavelli, R. W. MacLeod, G. Schmid, F. S. Stephens, K. Vetter, R. Wadsworth, and S. Frauendorf, Phys. Rev. Lett. **78**, 1868 (1997).
[9] R. M. Clark and A. O. Macchiavelli, Annu. Rev. Nucl. Part. Sci. **50**, 1 (2000).
[10] S. Frauendorf, Nucl. Phys. **A557**, 259c (1993).
[11] S. Frauendorf, J. Meng, and J. Reif (unpublished).
[12] S. Frauendorf, Z. Phys. A **358**, 163 (1997).

[13] A. Gadea, G. de Angelis, C. Fahlander, M. De Poli, E. Farnea, T. Li, D. R. Napoli, Q. Pan, P. Spolaore, D. Bazzacco, S. M. Lenzi, S. Lunardi, C. M. Petrache, F. Brandolini, P. Pavan, C. Rossi-Alvarez, S. Sferrazza, P. G. Bizetti, A. M. Bizetti Sona, J. Nyberg, M. Lipoglavsek, J. Persson, J. Cederkäll, D. Seweryniak, A. Johnson, H. Grawe, F. Soramel, M. Ogawa, A. Makishima, R. Schubart, and S. Frauendorf, Phys. Rev. C **55**, R1 (1997).
[14] S. Frauendorf and J. Reif, Nucl. Phys. **A621**, 736 (1997).
[15] D. G. Jenkins, I. M. Hibbert, C. M. Parry, R. Wadsworth, D. B. Fossan, G. J. Lane, J. M. Sears, J. F. Smith, R. M. Clark, R. Krücken, I. Y. Lee, A. O. Macchiavelli, V. P. Janzen, J. Cameron, and S. Frauendorf, Phys. Lett. B **428**, 23 (1998).
[16] D. G. Jenkins, R. Wadsworth, J. Cameron, R. M. Clark, D. B. Fossan, I. M. Hibbert, V. P. Janzen, R. Krücken, G. J. Lane, I. Y. Lee, A. O. Macchiavelli, C. M. Parry, J. M. Sears, J. F. Smith, and S. Frauendorf, Phys. Rev. C **58**, 2703 (1998).
[17] R. M. Clark, S. J. Asztalos, B. Busse, C. J. Chiara, M. Cromaz, M. A. Deleplanque, R. M. Diamond, P. Fallon, D. B. Fossan, D. G. Jenkins, S. Juutinen, N. Kelsall, R. Krücken, G. J. Lane, I. Y. Lee, A. O. Macchiavelli, R. W. McLeod, G. Schmid, J. M. Sears, J. F. Smith, F. S. Stephens, K. Vetter, R. Wadsworth, and S. Frauendorf, Phys. Rev. Lett. **82**, 3220 (1999).
[18] F. Brandolini, M. Ionescu-Bujor, N. H. Medina, R. V. Ribas, D. Bazzacco, M. De Poli, P. Pavan, C. Rossi-Alvarez, G. de Angelis, S. Lunardi, D. De Acuña, D. R. Napoli, and S. Frauendorf, Phys. Lett. B **388**, 468 (1996).
[19] H. Schnare, R. Schwengner, S. Frauendorf, F. Dönau, L. Käubler, H. Prade, A. Jungclaus, K. P. Lieb, C. Lingk, S. Skoda, J. Eberth, G. de Angelis, A. Gadea, E. Farnea, D. R. Napoli, C. A. Ur, and G. Lo Bianco, Phys. Rev. Lett. **82**, 4408 (1999).
[20] R. Schwengner, H. Schnare, S. Frauendorf, F. Dönau, L. Käubler, H. Prade, E. Grosse, A. Jungclaus, K. P. Lieb, C. Lingk, S. Skoda, J. Eberth, G. de Angelis, A. Gadea, E. Farnea, D. R. Napoli, C. A. Ur, and G. Lo Bianco, J. Res. Natl. Inst. Stand. Technol. **105**, 133 (2000).
[21] D. Bazzacco (unpublished).
[22] D. C. Radford, Nucl. Instrum. Methods Phys. Res. A **361**, 297 (1995).
[23] J. Theuerkauf, S. Esser, S. Krink, M. Luig, N. Nicolay, and H. Wolters, program vs (version 6.65), Universität zu Köln, 1992.
[24] R. M. Steffen and K. Alder, in *The Electromagnetic Interaction in Nuclear Spectroscopy*, edited by W. D. Hamilton (North-Holland, Amsterdam, 1975), p. 505.
[25] K. S. Krane, R. M. Steffen, and R. M. Wheeler, Nucl. Data Tables **11**, 351 (1973).
[26] A. Krämer-Flecken, T. Morek, R. M. Lieder, W. Gast, G. Hebbinghaus, H. M. Jäger, and W. Urban, Nucl. Instrum. Methods Phys. Res. A **275**, 333 (1989).
[27] G. Winter, Nucl. Instrum. Methods **214**, 537 (1983).
[28] J. Lindhard, V. Nielsen, and M. Scharff, Mat. Fys. Medd. K. Dan. Vidensk. Selsk. **36**, 1 (1968).
[29] G. Winter, J. Döring, F. Dönau, and L. Funke, Z. Phys. A **334**, 415 (1989).
[30] R. Schwengner, J. Döring, L. Funke, H. Rotter, G. Winter, A. Johnson, and A. Nilsson, Nucl. Phys. **A486**, 43 (1988).
[31] J. Döring, L. Funke, W. Wagner, and G. Winter, Z. Phys. A **339**, 425 (1991).
[32] J. Döring, D. Ulrich, G. D. Johns, M. A. Riley, and S. L. Tabor, Phys. Rev. C **59**, 71 (1999).
[33] P. M. Endt, At. Data Nucl. Data Tables **23**, 547 (1979).
[34] J. Döring, G. Winter, L. Funke, L. Käubler, and W. Wagner, Z. Phys. A **338**, 457 (1991).
[35] G.-B. Han, S.-X. Wen, X.-G. Wu, X.-A. Liu, G.-S. Li, G.-J. Yuan, Z.-H. Peng, P.-K. Weng, C.-X. Yang, Y.-J. Ma, and J.-B. Lu, Chin. Phys. Lett. **16**, 487 (1999).
[36] D. Zwarts, Comput. Phys. Commun. **38**, 365 (1985).
[37] R. Schwengner, G. Winter, J. Reif, H. Prade, L. Käubler, R. Wirowski, N. Nicolay, S. Albers, S. Eßer, P. von Brentano, and W. Andrejtscheff, Nucl. Phys. **A584**, 159 (1995).
[38] R. Schwengner, J. Reif, H. Schnare, G. Winter, T. Servene, L. Käubler, H. Prade, M. Wilhelm, A. Fitzler, S. Kasemann, E. Radermacher, and P. von Brentano, Phys. Rev. C **57**, 2892 (1998).
[39] G. Winter, R. Schwengner, J. Reif, H. Prade, L. Funke, R. Wirowski, N. Nicolay, A. Dewald P. von Brentano, H. Grawe, and R. Schubart, Phys. Rev. C **48**, 1010 (1993).
[40] G. Winter, R. Schwengner, J. Reif, H. Prade, J. Döring, R. Wirowski, N. Nicolay, P. von Brentano, H. Grawe, and R. Schubart, Phys. Rev. C **49**, 2427 (1994).
[41] J. Reif, G. Winter, R. Schwengner, H. Prade, and L. Käubler, Nucl. Phys. **A587**, 449 (1995).
[42] E. A. Stefanova, R. Schwengner, J. Reif, H. Schnare, F. Dönau, M. Wilhelm, A. Fitzler, S. Kasemann, P. von Brentano, and W. Andrejtscheff, Phys. Rev. C **62**, 054314 (2000).
[43] A. Jungclaus, D. Kast, K. P. Lieb, C. Teich, M. Weiszflog, T. Härtlein, C. Ender, F. Köck, D. Schwalm, J. Reif, R. Peusquens, A. Dewald, J. Eberth, H. G. Thomas, M. Górska, and H. Grawe, Nucl. Phys. **A637**, 346 (1998).
[44] A. Jungclaus, D. Kast, K. P. Lieb, C. Teich, M. Weiszflog, T. Härtlein, C. Ender, F. Köck, D. Schwalm, I. P. Johnstone, J. Reif, R. Schwengner, R. Peusquens, A. Dewald, J. Eberth, H. G. Thomas, M. Górska, and H. Grawe, Phys. Rev. C **60**, 014309 (1999).
[45] E. A. Stefanova, R. Schwengner, G. Rainovski, K. D. Schilling, A. Wagner, F. Dönau, E. Galindo, A. Jungclaus, K. P. Lieb, O. Thelen, J. Eberth, D. R. Napoli, C. A. Ur, G. de Angelis, M. Axiotis, A. Gadea, N. Marginean, T. Martinez, Th. Kröll, and T. Kutsarova, Phys. Rev. C **63**, 064315 (2001).
[46] E. A. Stefanova, M. Danchev, R. Schwengner, D. L. Balabanski, M. P. Carpenter, M. Djongolov, S. M. Fischer, D. J. Hartley, R. V. F. Janssens, W. F. Mueller, D. Nisius, W. Reviol, L. L. Riedinger, and O. Zeidan, Phys. Rev. C **65**, 034323 (2002).
[47] X. Ji and B. H. Wildenthal, Phys. Rev. C **37**, 1256 (1988).
[48] R. Gross and A. Frenkel, Nucl. Phys. **A267**, 85 (1976).
[49] J. Blomqvist and L. Rydström, Phys. Scr. **31**, 31 (1985).
[50] D. H. Gloeckner and F. J. D. Serduke, Nucl. Phys. **A220**, 477 (1974).
[51] S. Frauendorf, J. Reif, and G. Winter, Nucl. Phys. **A601**, 41 (1996).